Thermoelectric transport and phonon drag in Weyl semimetal monochalcogenides

Xitong Xu,[1,2] Yiyuan Liu,[1] Gabriel Seyfarth,[3,4] Alexandre Pourret,[5] Wenlong Ma,[1] Huibin Zhou,[1] Guangqiang Wang,[1] Zhe Qu,[2,6] and Shuang Jia[1,7,8,9,*]

[1]*International Center for Quantum Materials, School of Physics, Peking University, Beijing 100871, China*
[2]*Anhui Key Laboratory of Condensed Matter Physics at Extreme Conditions, High Magnetic Field Laboratory, HFIPS, Chinese Academy of Sciences, Hefei, Anhui 230031, China*
[3]*Université Grenoble Alpes, Grenoble F-38000, France*
[4]*Laboratoire National des Champs Magnetiques Intenses (LNCMI-EMFL), CNRS, UGA, UPS, INSA, Grenoble F-38042, France*
[5]*Université Grenoble Alpes, CEA, INAC-PHELIQS, Grenoble F-38000, France*
[6]*CAS Key Laboratory of Photovoltaic and Energy Conservation Materials, Hefei Institutes of Physical Sciences, Chinese Academy of Sciences, Hefei, Anhui 230031, China*
[7]*Interdisciplinary Institute of Light-Element Quantum Materials and Research Center for Light-Element Advanced Materials, Peking University, Beijing 100871, China*
[8]*Collaborative Innovation Center of Quantum Matter, Beijing 100871, China*
[9]*CAS Center for Excellence in Topological Quantum Computation, University of Chinese Academy of Sciences, Beijing 100190, China*

(Received 15 April 2021; revised 26 July 2021; accepted 8 September 2021; published 29 September 2021)

The topological effect in thermoelectric transport is an important research aspect in semimetals, but whether an anomalous Nernst effect exists in nonmagnetic topological semimetals in a finite external field is still under debate. To demonstrate how to discern the topological effect in nonmagnetic topological semimetals, we present a comprehensive study on the magnetothermoelectric properties for four Weyl semimetals: TaAs, TaP, NbAs, and NbP. We observe large magneto-Seebeck and Nernst signals at intermediate temperatures, which are attributed to a multiband ordinary contribution and an inelastic, phonon-drag effect, while the latter is ignored in previous studies. This phonon-drag effect also induces an unusual, prominent temperature and field dependence of quantum oscillations in thermoelectric transport signals. On the other hand, only signatures of a relatively small anomalous thermoelectric effect are found in TaAs compared with the ordinary effect.

DOI: 10.1103/PhysRevB.104.115164

I. INTRODUCTION

Thermoelectricity describes a phenomenon in which charge flows are inevitably accompanied by entropy flows, and vice versa. The potential of this heat-electricity conversion has inspired numerous experimental and theoretical attempts, including perhaps the most successful material realization, namely bismuth telluride and its alloys [1]. Moreover, as a probe for physical phenomena related with energy change, thermoelectric measurement has the sensitivity preceding ordinary electric transport, which is guaranteed by the widely known Mott formula [2], $\boldsymbol{\alpha} = \frac{\pi^2}{3}\frac{k_B^2 T}{e}\frac{\partial \boldsymbol{\sigma}}{\partial \epsilon}|_{\epsilon_F}$, where $\boldsymbol{\alpha}$ and $\boldsymbol{\sigma}$ are the thermoelectric and electric conductivity tensor, respectively.

The thermoelectrical properties of various topological materials are receiving renewed interest now, especially when they are under a magnetic field [3–10]. One of the research focuses is the quantum oscillations (QOs) of magnetothermoelectric signals, which are adapted to map the Fermi surfaces for various topological materials because their sensitivity is much better than that of Shubnikov–de Haas oscillations in resistivity [11–14]. Profound topological effects have been proposed in thermoelectricity in Dirac and Weyl semimetals, including the anomalous Nernst effect (ANE) stemming from the nonzero Berry curvature in nonmagnetic compounds in a finite external magnetic field [7,15,16]. It is also proposed that the linearly dispersive bands in Dirac and Weyl semimetals will result in a nonsaturating magnetothermopower and "quantized" thermoelectric Hall conductivity in the dissipationless limit at low temperature and high magnetic field [9,10].

Nevertheless, studies on the thermoelectric properties of matter are complicated by several aspects. In practice, the thermopower $\boldsymbol{S}$ (rather than the fundamental $\boldsymbol{\alpha}$) for a material is usually measured as the voltage generated by a thermal gradient at different temperatures and magnetic fields. The total $\boldsymbol{S}$ for a multiband system is the weighted average of every band,

$$\boldsymbol{S} = \sum_i \sigma_i \boldsymbol{S}_i \Big/ \sum_i \sigma_i, \tag{1}$$

where the subscript i denotes different bands. The magnetoresponse of the entangled thermopower can be complex for systems with multiple carriers since it is related with the electric conductivity as well. Proper consideration of the multiband effect is needed when discerning topological

*gwljiashuang@pku.edu.cn

effects, for instance the ANE from the ordinary effect in topological semimetals.

The inelastic process is another important thermoelectric driven force in semimetals. In a thermally equilibrated solid, lattice vibrations often act as elastic scattering centers for the drifting electrons under an electric field. When a solid is under a temperature gradient, the flows of charge carriers and phonon modes get entangled. Carrying both energy and momentum, the phonons drift along the established temperature gradient and scatter with electrons differently at the hot and cold end. This difference leads to extra charge flows effectively, and hence an additional electric voltage is generated as a part of total thermoelectric signals. Such an inelastic process is the so-called phonon-drag effect [1,17–19]. The additional thermopower (S_g) induced by phonon drag can be roughly estimated as [18,19]

$$S_g \sim \frac{C_L}{3ne}\eta, \tag{2}$$

where C_L is the lattice specific heat, n is the carrier density, and η is a parameter reflecting a phonon's scattering possibility with an electron. The formula indicates that phonon drag plays a significant role in semimetals and semiconductors with low carrier density. This part of the contribution has yet to be identified in topological semimetals.

The two ordinary effects listed above can significantly contribute to the magnetothermoelectric signals in topological semimetals. In this paper, we present a comprehensive study on the magnetothermoelectric transport properties for the four isostructural compounds in the Weyl semimetal TaAs family in order to demonstrate how we can effectively disentangle the ordinary and topological effects in Dirac and Weyl semimetals. TaAs, TaP, NbAs, and NbP are the prototype Weyl semimetals, possessing low-density, highly mobile electrons, and holes [5,20,21]. Due to different spin-orbital coupling strength, the Fermi energy and pockets of these four members have slight differences, which are, however, crucial for their topological electronic properties [22]. For instance, negative longitudinal magnetoresistance, as a result of a chiral anomaly for Weyl electrons, has been confirmed in TaAs [23,24], while contradictory observations were reported in other members whose Fermi surface surrounds pairs of Weyl points and the chirality is ill-defined [25–27]. A comparative study of the thermoelectric properties in this family can help us understand their difference and develop a strategy for weighing the topological and ordinary effects.

Previous experimental works reported the steplike feature in Nernst signals and the large thermoelectric response under magnetic field in the TaAs family. These features were attributed to topological origins in general [28–31]. In this work, we clarify a multiband effect in the thermoelectric properties which was inadequately considered in previous studies. The multiband effect leads to a large ordinary contribution which overwhelms the anomalous contribution in this family. We only discern signatures of anomalous thermoelectric Hall conductivity in TaAs, while the ANE is negligible for the other members in our measurements. While theoretical studies only consider the thermoelectricity in topological semimetals as electrons' diffusive response to an external electromagnetic field and a thermal gradient, we declare the existence of a phonon-drag contribution, and we emphasize its importance to the large Seebeck and Nernst effects. This inelastic effect also induces an unusual temperature and field dependence of QOs in thermoelectric signals. We also investigate the thermoelectricity in a high-field limit. The ordinary effect is found to outweigh the theoretically proposed topological effects, namely the nonsaturating magnetothermopower and "quantized" thermoelectric Hall conductivity, in the TaAs family.

This paper is organized as follows: The magnetic-field-dependent thermoelectrical signals (S_{xx} and S_{xy}) for the TaAs family at different temperatures are shown in Sec. III. We highlight two spectacular observations in the Nernst signals: (i) the steplike profile at low temperatures and the giant magnetic-field response at intermediate temperatures; and (ii) the sharp, sawlike QOs at high fields. In the first two subsections (Secs. IV A and IV B) of the Analysis part, we clarify that the steplike Nernst signals mainly stem from an ordinary, multiband effect of highly mobile carriers while a possible ANE contribution is only discerned in TaAs. In the next two subsections, we focus on the nonoscillatory components and QOs in thermoelectrical signals, respectively. We point out the significant role of the inelastic, phonon-drag effect. In Sec. IV E, we show the thermoelectric signals for TaAs and TaP under high magnetic field.

II. METHOD

Single crystals of TaAs, TaP, NbAs, and NbP were grown via the chemical vapor transport method [32–34]. Crystals were polished into a cuboid shape with a typical size of $2 \times 0.4 \times 0.15$ mm^3, corresponding to the crystallographic a, b, and c axis, respectively. All our samples are of high quality, showing low residual resistance and large magnetoresistance (see details in Figs. S1 and S2 in the Supplemental Material [35]). Thermoelectric measurements were carried out in a 14 T Oxford Teslatron PT system, with magnetic field parallel to the c axis and thermal gradient along a. Vacuum better than 5×10^{-5} Pa was maintained during the experiments. Angle-dependent thermoelectric measurements were done inside an indium-sealed capsule on a rotational probe. Electric measurements were performed on the same samples. To exclude the possibility of mixing up the longitudinal and transverse thermoelectric signals in an adiabatic setup [36], we also check the thermal Hall effect using a three-thermometer–one-heater setup. Because the phonon contribution dominates in thermal conductivity and the electron-hole is compensated, we see no significant Righi-Leduc coefficient at low temperatures (Fig. S4 in the Supplemental Material [35]). Hereafter, we do not distinguish between the isothermal and adiabatic thermopower as they are almost the same in this case. High-field measurement of TaP up to 35 T and down to 0.6 K was done in the high-field laboratory LNCMI-CNRS.

III. EXPERIMENTAL RESULTS

Figure 1 shows our spectacular findings for the thermoelectricity of the TaAs family under magnetic field at 2 K. The signals of S_{xx} and S_{xy} have a giant response to magnetic field and manifest much more profound QOs than those in electrical signals [see Fig. S1(a) in the Supplemental Material

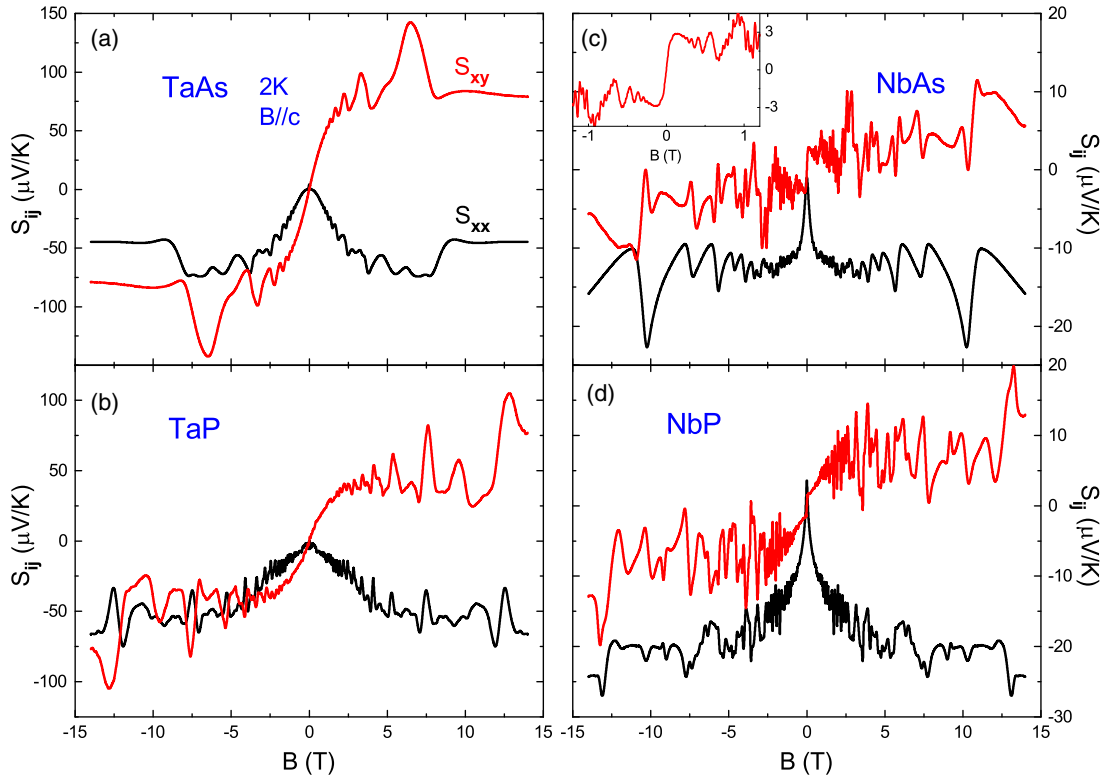

FIG. 1. (a)–(d) Thermoelectrical signals S_{ij} of TaAs, TaP, NbAs, and NbP at 2 K, respectively. Note the different scales. All these profiles feature strong QOs. Inset in (c): Zoom-in of S_{xy} of NbAs under small magnetic field, showing a sharp steplike behavior and QOs with ultralow frequency.

[35]]. In general, the nonoscillatory component of S_{xx} is gradually saturated at high field while the Nernst thermopower S_{xy} shares a steplike profile. The steplike feature is more evident in NbAs and NbP [see Fig. 1(c), inset], reminding us of the reported ANE in Cd_3As_2 [7]. In Sec. IV A we prove that the profile of S_{xy} in the TaAs family is due to a multiband effect stemming from multitype, highly mobile carriers, similar to those observed in bismuth and graphite [41,42].

It is noteworthy that the S_{xy} is superposed with sharp, sawlike QOs at high field, and the oscillatory amplitudes are comparable to the nonoscillating background. Large QOs with asymmetric peaks in Nernst signals were also reported in bismuth and graphite [41,42], which is ascribed to the effect of the last few Landau levels evacuating a three-dimensional (3D) Fermi surface (FS) at low temperatures [43,44]. Below we show that phonon drag plays an important role in these QOs in the TaAs family under high magnetic field. Preliminary analysis of the QO parameters is shown in Sec. C in the Supplemental Material [35], and the main result is summarized in Table I.

Figure 2 shows S_{xx} and S_{xy} at elevated temperatures. Both S_{xx} and S_{xy} retain a saturating profile below 50 K, and then they develop into a quasilinear profile and decay quickly above 150 K. Similar to the previous reports [28,29,31], we also observed giant magneto-thermoelectric power at intermediate temperatures. The maximum values of S_{xx} and S_{xy} in the TaAs family are all in the order of 1 mV/K. These values are comparable with those for traditional thermoelectric materials in low field, like $Bi_2Te_{2.1}Se_{0.9}$ (400 μV/K at 100 K [45]) and InSb (1.3 mV/K at 1.85 T, 100 K) [46,47]. We also notice some semimetals having a large response of more than 1 mV/K, including bismuth [48], graphite [42], and WTe_2 [49]. Highly mobile carriers with a small Fermi energy can generate a large S_{xx} in semimetals, while an additional electron-hole compensation can lead to a large ordinary S_{xy} [50]. In topological semimetals, the Berry curvature field can also contribute an anomalous term in S_{xy} [15,16], which is discussed in the next section. We also demonstrate that the phonon drag in the TaAs family plays an important role in the giant magnetothermoelectric power at intermediate temperatures.

IV. ANALYSIS AND DISCUSSION

A. Ordinary and anomalous contribution in thermoelectricity

The Nernst response can constitute two components, the ordinary and the anomalous. The former depends on quasiparticle transport, and it can vary tremendously in magnitude for different carrier mobilities and corresponding Fermi energies [18,19]. The anomalous Nernst response, on the other hand, can be regarded as a topological effect because the Berry curvature $\Omega(\boldsymbol{k})$ imparts to the carriers an anomalous velocity $v_A = \Omega(\boldsymbol{k}) \times \hbar\dot{\boldsymbol{k}}$ [51]. When time-reversal symmetry is broken, Berry curvature across surfaces acquires nonzero momentum space integrals in the Brillouin zone, leading to the nonvanishing anomalous Hall effect (AHE) and ANE. This could be achieved in magnetic systems spontaneously, or in a nonmagnetic Dirac/Weyl system in the presence of an external magnetic field [7,15]. Previous theoretical study on a fictitious inversion symmetry-breaking Weyl semimetal

TABLE I. A summary of transport properties in the TaAs family. For NbAs and NbP, only the main frequencies with the smallest cyclotron masses are listed because the light carriers easily respond to entropy changes. Data for bismuth are reproduced from Ref. [72], and are listed for comparison. Θ_D is from Refs. [70,71]. Θ_D^* is calculated via assuming equal longitudinal and transverse sound velocity.

	TaAs	TaP	NbAs	NbP	Bi
k_F (nm^{-1})	0.146(7 T)	0.235(18 T)	0.202(13.5 T)	0.302(30.1 T)	0.14
m^* (m_e)	0.14	0.11	0.09	0.14	0.06
ϵ_F (meV)	11.5	38.6	35.5	50.0	27
μ ($m^2/V\,s$)	55	8.5	34	50	420
$\frac{\pi^2}{3}\frac{k_B^2}{e}\frac{\mu}{\epsilon_F}$ ($\mu V/K^2\,T$)	108	5.4	23.4	14	383
ν/T ($\mu V/K^2\,T$)	28.6(2 K)	10.6(1 K)	19.1(2 K)	6.7(2 K)	750(0.3 K)
Θ_D (K)	341	408	409	515	120
Θ_D^* (K)	6.6	12.3	11.0	20.0	3.0

suggests that the anomalous Nernst contribution has a much smaller magnitude than that of the conventional part [16].

The ANE caused by nonvanishing Berry curvature of electrons is now a mature field of research in ferromagnetic materials. It has been observed in several magnetic compounds like Mn_3Sn [52], Mn_3Ge [53], Co_2MnGa [54,55], $Co_3Sn_2S_2$ [56,57], and Fe_3Sn_2 [58]. Theoretical calculations of the Berry curvature predict the rough magnitude of the anomalous Hall conductivity, and ANE data can be comparable. On the other hand, the ANE are less sufficiently studied in nonmagnetic topological materials like $ZrTe_5$ [59,60], Cd_3As_2 [7], and the TaAs family. The multiband effect can give rise to a steplike profile in S_{xy} [41,42] in a finite magnetic field, which may complicate the observed Nernst signals in Weyl semimetals. Therefore, we need a criterion to judge whether the ANE exist in general and to distinguish the anomalous part from the ordinary one in the TaAs family.

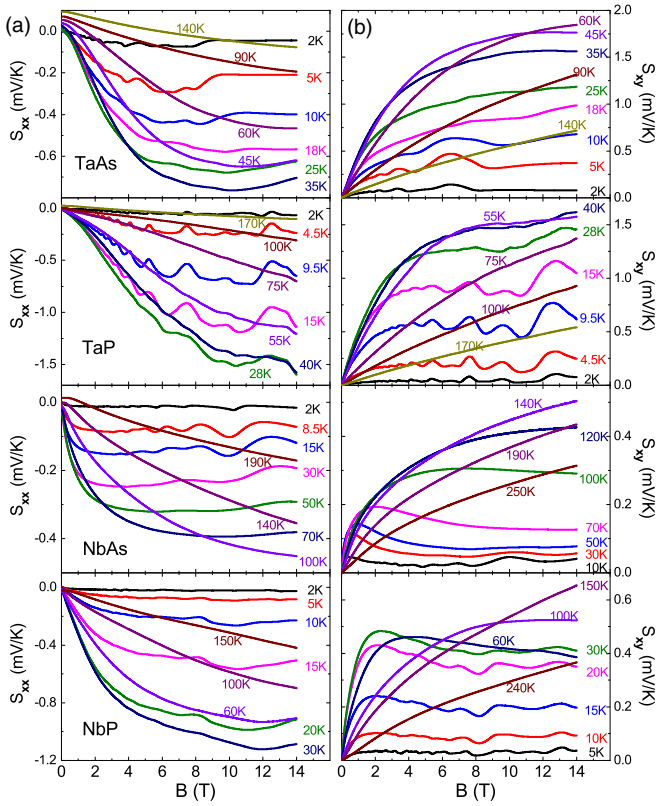

FIG. 2. (a) S_{xx} and (b) S_{xy} for the TaAs family at selected temperatures. The maximal values are in the order of 1 mV/K. Note the saturating profile of S_{xx} and S_{xy} under high magnetic field.

Our strategy is to calculate the thermoelectric tensor $\boldsymbol{\alpha}$ from the derived quantity $\boldsymbol{S} = \boldsymbol{\alpha}/\boldsymbol{\sigma}$ and then discern the anomalous contribution from the off-diagonal component α_{xy}, namely the thermoelectric Hall conductivity. This term is more fundamental, and contributions of different origins can be separated immediately. α_{xy} can be formulated as [15,16]

$$\alpha_{xy} = \alpha_{xy}^N + \alpha_{xy}^A. \tag{3}$$

The first term on the right side represents the conventional term, which can be expressed as [19]

$$\alpha_{xy}^N = -\frac{\alpha_e^0 \mu_e B}{1+\mu_e^2 B^2} + \frac{\alpha_h^0 \mu_h B}{1+\mu_h^2 B^2} \tag{4}$$

for a compensated semimetal within the semiclassical region. Here $\mu_{e/h}$ denotes the carrier mobility of an electron/hole, and $\alpha_{e/h}^0$ denotes the zero-field value, which is negative/positive for electrons and holes, respectively. Note the normal part includes both diffusive and phonon-drag contributions. It is clear that α_{xy}^N is dominated by the contribution from highly mobile carriers. Typically it will peak around $\mu B \sim 1$ and approach zero when $\mu B \gg 1$. The effect of Landau quantization and the correction in the high-field limit are discussed in Secs. IV D and IV E, respectively.

The second term in Eq. (3) is the anomalous contribution from Berry curvature $\Omega_{\boldsymbol{k}}$ which is saturating in a small external field,

$$\alpha_{xy}^A = \frac{e k_B}{\hbar} \int d\boldsymbol{k}\, \Omega_z\, s_{\boldsymbol{k}}, \tag{5}$$

where $s_{\boldsymbol{k}} = -f_{\rm eq}\ln f_{\rm eq} - (1-f_{\rm eq})\ln(1-f_{\rm eq})$ is the entropy density function [15,16], and $f_{\rm eq}$ is the equilibrium Fermi-Dirac distribution.

To discern the ANE, we plot α_{xy} versus magnetic field for the TaAs family at 40 K in Fig. 3(b), where S_{xy} shows the most prominent plateaulike profile [Fig. 3(a)]. The thermoelectric Hall conductivity increases steeply at low field and peaks when $\mu_0 H < 0.5$ T. In higher magnetic field, α_{xy} approaches zero, which is a clear semiclassical feature for

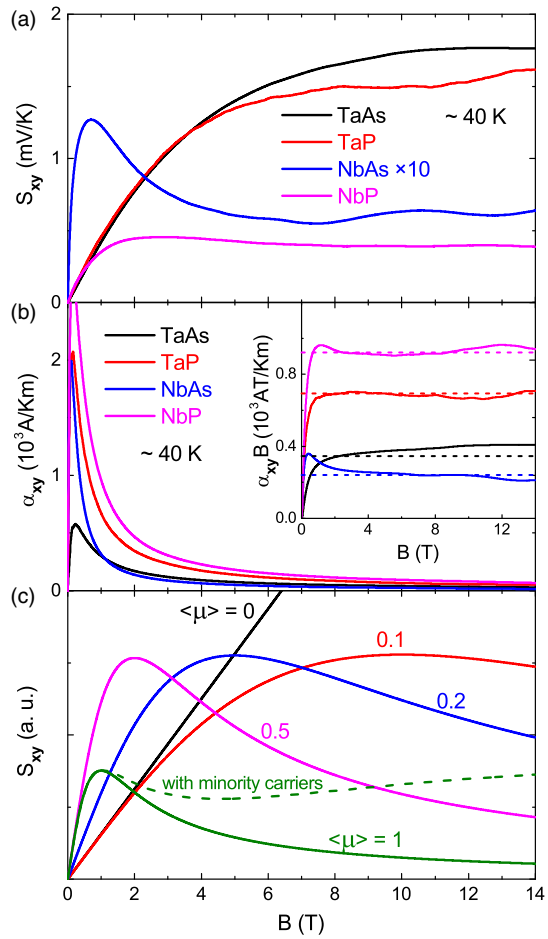

FIG. 3. (a) S_{xy} for the TaAs family at about 40 K. For NbAs there is 10 times magnification. (b) The off-diagonal component of the thermoelectric tensor α_{xy} for the TaAs family at 40 K. All curves approach zero in high magnetic field. Inset: corresponding $\alpha_{xy}B$. The horizontal dashed lines are a guide to the eye. (c) A simulation of S_{xy} using the two-band model. Here μ is set to be 40 and 10 $m^2/V\,s$ for electrons and holes, respectively. Total carrier concentration $(n_e + n_h)$ is set to be 10^{19} cm^{-3}. α_0 is set to be equal for electrons and holes. The dashed line shows the modified S_{xy} in high field when a third minority carrier is considered. Here we assume the third carrier having 10^{18} cm^{-3} carrier density and 0.03 $m^2/V\,s$ mobility.

highly mobile carriers. Therefore, we conclude that the normal term dominates the total α_{xy} in the TaAs family, and the plateaulike profiles of S_{xy} in Fig. 3(a) are *not* a manifestation of ANE.

Some numeric simulations can help us to better understand how the multiband effect results in the plateaulike profile in S_{xy} in compensated semimetals. If we consider a complex representation of the two-band model,

$$\begin{aligned}\widehat{\sigma} &= -\frac{n_e e\mu_e}{1+i\mu_e B} - \frac{n_h e\mu_h}{1-i\mu_h B},\\ \widehat{\alpha} &= \frac{\alpha_e^0}{1+i\mu_e B} + \frac{\alpha_h^0}{1-i\mu_h B},\end{aligned} \tag{6}$$

and $\widehat{S} = \widehat{\alpha}/\widehat{\sigma}$, one can calculate with ease (Sec. E in the Supplemental Material [35]) that

$$S_{xy} \propto \frac{B}{1+\langle\mu\rangle^2 B^2}, \tag{7}$$

where $\langle\mu\rangle = |n_e - n_h|\mu_e\mu_h/(n_e\mu_e + n_h\mu_h)$. We notice that the profile of S_{xy} depends on the averaged mobility $\langle\mu\rangle$ instead of μ_e or μ_h alone [49,61]. For a perfect compensation of electrons and holes, namely $\langle\mu\rangle$ equaling zero, a linear S_{xy} is expected. When $\langle\mu\rangle$ gradually increases, a maximum value occurs at the field equaling $1/\langle\mu\rangle$. This peak can be very broad if $\langle\mu\rangle$ is close to zero. By varying $\langle\mu\rangle$ between 0 and 1 $m^2/V\,s$, we roughly reproduce the profiles of S_{xy} for the TaAs family in Fig. 3(c). Moreover, additional contribution from other less mobile carriers can make the profile of S_{xy} more like a plateau in a finite magnetic field. The dashed line in Fig. 3(c) represents S_{xy} for $\langle\mu\rangle = 1$ $m^2/V\,s$, which is further modified by a third carrier. We notice that the dashed line is similar to the profile of S_{xy} in NbP and NbAs at intermediate temperatures to a higher extent. Our simulation of S_{xy} in a fictitious multiband system indicates that the plateaulike profile can be attributed to a collaborative effect of multicarriers with reasonable parameters, and therefore the analysis on α_{xy} is necessary for discerning the anomalous effect in thermoelectricity in nonmagnetic materials.

Now we try to figure out whether there exists discernible α_{xy}^A in the total α_{xy}. Noticing that the TaAs family has highly mobile electrons and holes whose mobilities are much larger than 1 $m^2/V\,s$ [Fig. S1(c)] below 100 K, we consider α_{xy} in a high-field limit,

$$\alpha_{xy}B \simeq \left(-\frac{\alpha_e^0}{\mu_e} + \frac{\alpha_h^0}{\mu_h}\right) + \alpha_{xy}^A B. \tag{8}$$

This equation gives us a criterion to address a nonzero anomalous term as a finite linear slope in $\alpha_{xy}B$ at the high-field limit for nonmagnetic semimetals. As shown in the inset in Fig. 3(b), all four members possess a nearly constant $\alpha_{xy}B$ above 1 T. At 40 K and 10 T, the greatest anomalous contribution in S_{xy} is estimated to be around 10% in TaAs. Our result is consistent with theoretical calculation in Ref. [16], which claims that the conventional Nernst response dominates over the anomalous one in nonmagnetic Weyl semimetals.

B. Possible anomalous thermoelectric effect in TaAs

We now try to extract the plausible anomalous thermoelectric Hall conductivity term of TaAs which is directly related with the Berry curvature. Figure 4(a) shows $\alpha_{xy}B/T$ for TaAs at different temperatures. We can discern a small but apparent linear dependence of the nonoscillating background of $\alpha_{xy}B/T$ below 50 K, which is attributed to the anomalous term α_{xy}^A/T according to Eq. (8). This slope is close to zero at 2 K and quickly reaches a maximum value of 0.45 $A/K^2\,m$ at around 10 K, and then damps above 20 K [Fig. 4(b)]. Although α_{xy}^A in TaAs is only a fraction in total α_{xy} at low field, we note that the absolute value (~6.7 A/K m at 15 K) is larger than that of Fe (~0.2 A/K m [62]), and it is comparable to those in magnetic Weyl semimetals Co_2MnGa (~4 A/K m [54]) and $Co_3Sn_2S_2$ (~11 A/K m [56]).

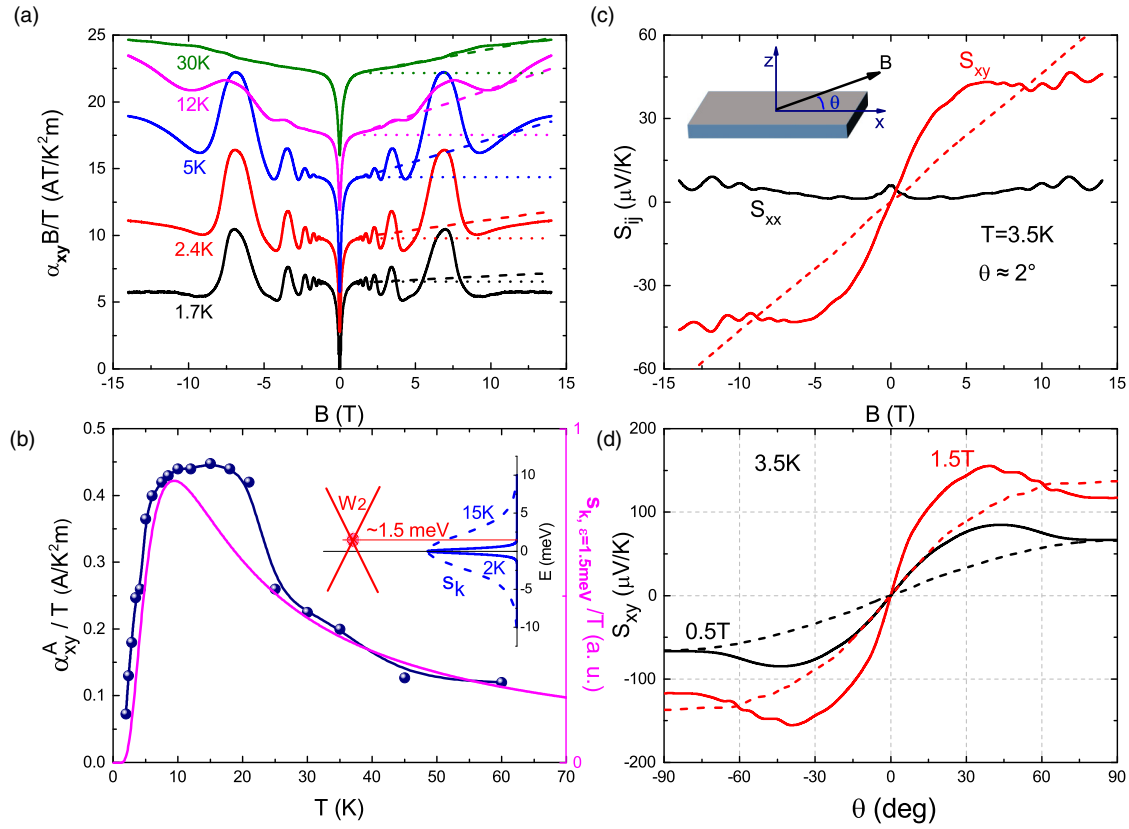

FIG. 4. (a) $\alpha_{xy}B/T$ at selected temperatures for TaAs. Curves are shifted vertically for clarity. A linear slope with field as depicted by the dashed line is observed above 1 T, indicating the existence of a small but sizable anomalous contribution. (b) Extracted anomalous thermoelectric Hall conductivity α^A_{xy}/T. The magenta line is the entropy density function $s_{\boldsymbol{k}}$ at 1.5 meV, divided by temperature. We notice that both plots reach maximal in the vicinity of a characteristic temperature $0.55\epsilon_F/k_B \simeq 10$ K. Inset: $s_{\boldsymbol{k},\epsilon=1.5\,\mathrm{meV}}$ at 2 and 15 K, and a sketch of W_2 nodes which are 1.5 meV above the Fermi level of TaAs. (c) Thermopower of TaAs when magnetic field is almost along the a axis (about 2°) at 3.5 K. The longitudinal part S_{xx} varies little with field, while the transverse component S_{xy} has a large, plateaulike feature. The red dashed line shows the expected S_{xy} inferred from S_{xy} at $\theta = 90°$, assuming only the field component along c contributes to transport signals. (d) Angle-dependent S_{xy} at 3.5 K under a field of 0.5 and 1.5 T, respectively. Dashed lines are also the semiclassically expected S_{xy}.

The broad maximum of α^A_{xy}/T at around 15 K in Fig. 4(b) can be readily explained if we consider the Berry curvature field Ω_z and the temperature dependence of the entropy density function $s_{\boldsymbol{k}}$ in Eq. (5). The Berry curvature field maximizes at 1.5 meV, corresponding to a thermal excitation about 15 K, as the Weyl nodes lie around this Fermi energy in TaAs [23,37]. Well below this temperature, $s_{\boldsymbol{k}}$ is like a δ-function which is misaligned with the hot spot of Berry curvature, and therefore α^A_{xy} is small. Above 15 K, $s_{\boldsymbol{k}}$ is fully extended in the energy scale, and α^A_{xy} intends to be saturating, leading to a damped α^A_{xy}/T with increasing temperature. We notice that $s_{\boldsymbol{k}}/T$ at 1.5 meV shows good consistency with the profile of α^A_{xy}/T [Fig. 4(b)]. As a comparison, we cannot discern sizable anomalous terms for TaP, NbAs, and NbP (see the details in Fig. S6 of the Supplemental Material [35]) below 50 K. The absence of the ANE for these three compounds seems to be consistent with the fact that the Fermi energies of their Weyl nodes are much larger than this energy scale.

To disentangle the anomalous and ordinary Nernst effect in TaAs, we also measured the thermoelectric signals when the magnetic field is slightly tilted (about 2°) with respect to the direction of applied temperature gradient [Fig. 4(c)]. In such a small angle, S_{xx} is very small while S_{xy} has already shown a plateaulike field dependence. Because the ordinary Nernst effect can only be generated by a perpendicular field component in the small angle, it is suppressed to be a quasilinear function, as illustrated by the dashed line in Fig. 4(c). In contrast, the α^A_{xy} which depends on the Berry curvature is less influenced by the direction of magnetic field. The observed plateaulike S_{xy} deviates greatly from the ordinary effect, demonstrating the possible existence of the ANE in TaAs. We also measured the angle dependence of S_{xy} when fixed magnetic fields (1.5 and 3 T) tilt away from the direction of applied temperature gradient [Fig. 4(d)]. The sharp switching near 0° in the angular dependence of S_{xy} indicates the existence of the anomalous term as well. A similar angular dependence has also been reported in the anomalous Hall effect in $ZrTe_5$ [59,63].

It is noteworthy that we do not resolve an AHE in the TaAs family in experiment (Fig. S1) and therefore we cannot compare two anomalous effects, as was done for magnetic Weyl semimetals [55,57]. It was suggested that Berry curvature induced $\alpha^A_{xy}/\sigma^A_{xy}$ should be a fraction of k_B/e at low temperatures for topological magnets [55,57]. However, we notice that the ratio of two anomalous terms for nonmagnetic topological semimetals seems to be much larger. The ratio of $\alpha^A_{xy}/\sigma^A_{xy}$ for

$ZrTe_5$ is close to k_B/e at 8 K [59] and soon surpasses this value at higher temperatures, considering a usually T-linear α_{xy}^A and T-independent σ_{xy}^A. In bulk Cd_3As_2, where a large ANE has also be observed [7], no AHE is reported to the best of our knowledge. The underlying cause behind this difference needs future studies.

C. Phonon-drag effect

In this section, we try to understand the large thermoelectric responses in the TaAs family at intermediate temperatures. We start from the signature of phonon drag at zero field and then identify its contribution in magnetothermoelectric signals.

According to the Mott relation [2,64], a T-linear behavior is expected for the diffusive Seebeck coefficient for one type of carrier at low temperatures,

$$S_d = \frac{\pi^2}{3}\frac{k_B}{e}\frac{k_B T}{\epsilon_F}(q+p), \tag{9}$$

where q equals 3/2 in 3D conditions, p equals $\frac{\partial \ln\tau}{\partial \ln\epsilon}|_{\epsilon_F}$, a value usually of the order of unity, depending on the detailed scattering process, and τ is the relaxation time. However, as shown in the inset of Fig. 5(a), an apparent deviation from linearity develops in the S_0 of TaAs at around 7 K. This hump is a typical signature of phonon drag as in semiconductors and semimetals such as germanium [65] and bismuth [66]. Using Eq. (2) and the value of C_L in Ref. [67], we estimate that the zero-field phonon-drag Seebeck coefficient S_g^0 is in the order of 10 μV/K around 10 K for TaAs, which is close in magnitude to the diffusive part in Eq. (9).

In TaP, NbP, and NbAs, however, no phonon-drag humps can be clearly resolved in S_0, due to the slightly higher carrier concentrations (see Fig. S1 in the Supplemental Material [35]) and the electron-hole compensation, which also leads to a sign change of S_0 at higher temperatures. To avoid the difficulty of discerning S_g from S_0, we now focus on the signals under a magnetic field alternatively. According to Refs. [64,68], the field dependence of inelastic $\boldsymbol{\alpha}^g$ is similar to diffusive $\boldsymbol{\alpha}^d$ when neglecting Landau quantization,

$$\boldsymbol{\alpha}^g = \frac{ne\mu}{1+\mu^2B^2}S_g^0, \tag{10}$$

which means that the phonon-drag effect can also be modulated by magnetic field. In particular, the Nernst effect measures the contribution from both electrons and holes instead of a cancellation between them, and S_{xx} approximates $\rho_{yx}\alpha_{xy}$ at low T and high fields. We therefore expect to see more features of phonon drag in magnetothermoelectric signals.

The Nernst coefficient ($\nu = \lim_{B\to 0} S_{xy}/B$) and magneto-Seebeck coefficient at a saturating field are shown in Figs. 5(b) and 5(c). For a single band [19],

$$\nu_d/T = -\frac{\pi^2}{3}\frac{k_B}{e}\frac{k_B}{\epsilon_F}\mu p. \tag{11}$$

This formula has enabled one to estimate the magnitude of the diffusive Nernst response in a given solid at low temperature given the mobility and the Fermi energy. In Fig. 6, the ν/T data for the TaAs family in the low-temperature limit all lie close to the empirical line of $283\mu/E_F$ by adapting the Fermi energy and mobility for dominant carriers, suggesting a qualitative agreement with Eq. (11). Note here that we have assumed $p \sim 1$, and to be more rigorous, a modified version of Eq. (11) (see the Supplemental Material, Sec. E [35]) may be better for a multiband system.

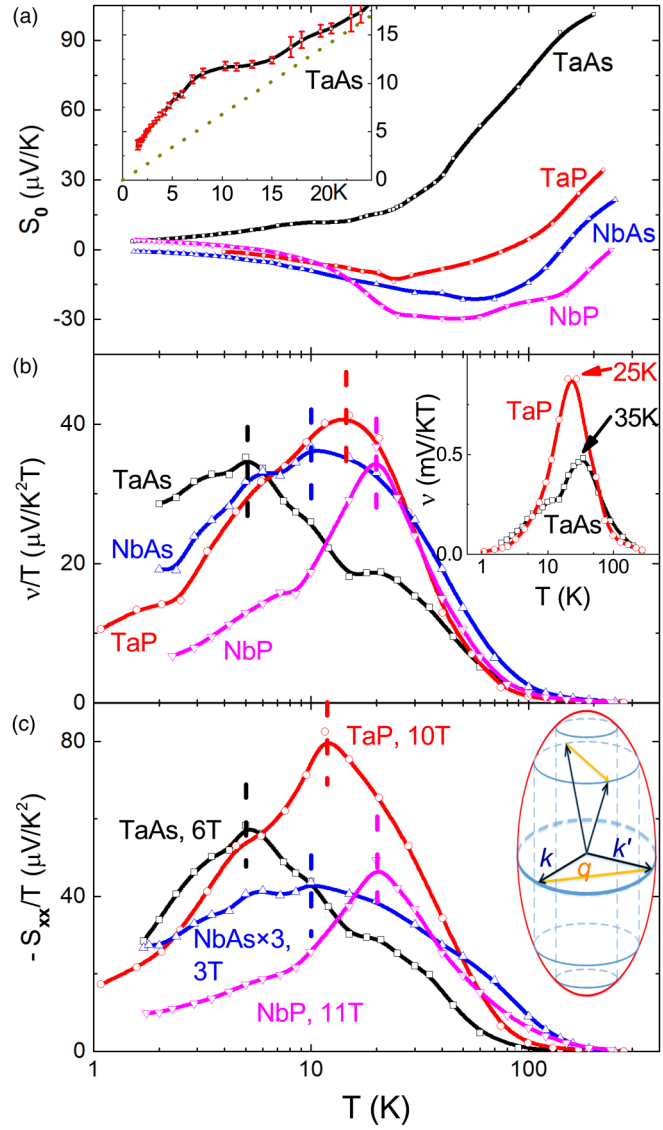

FIG. 5. (a) Zero-field Seebeck coefficient (S_0) for the TaAs family. Note the log temperature scale. Inset: zoom-in of S_0 for TaAs, showing a hump near 7 K. (b) Nernst coefficient divided by temperature (ν/T). We adopt $\nu = S_{xy}/B$ at 0.5 T for TaAs and TaP while 0.1 T for Nb siblings. Vertical dashed lines indicate peak positions, being ~5, 15, 10, and 20 K for TaAs, TaP, NbAs, and NbP, respectively. Inset: Corresponding ν for TaAs and TaP, showing peaks at 25 and 35 K, respectively. (c) $-S_{xx}/T$ vs temperature, showing a similar profile to ν/T in (b). For comparison, we select the magnetic field at which the low-temperature S_{xx} is saturated. The data for NbAs are magnified three times for clarity. Inset: a sketch for electron-phonon scattering N-process under a magnetic field. When colliding into a phonon with wave vector $\boldsymbol{q}$, the Fermi vector $\boldsymbol{k}$ changes its direction to $\boldsymbol{k}'$ while staying roughly on the Fermi sphere in the first Brillouin zone.

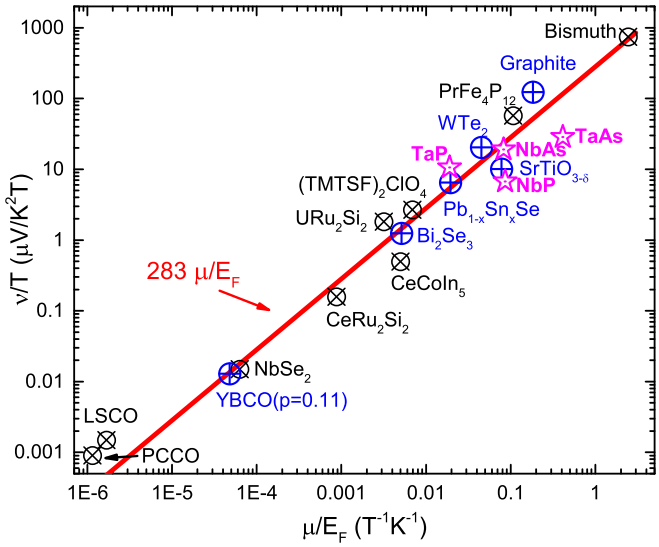

FIG. 6. Low-temperature Nernst coefficients divided by temperature (ν/T) in a variety of metals plotted vs the ratio of mobility to Fermi energy. The ν/T data for the TaAs family (magenta stars) in the low-temperature limit all lie close to the empirical line of $283\mu/E_F$. Black and blue data points are reproduced from Ref. [69].

Since the carrier mobility and concentration for the TaAs family remain almost intact below 50 K (Fig. S1 in the Supplemental Material), we expect the diffusive part of ν/T to be close to constant at low temperatures. In contrast, the value of ν/T for all four compounds is largely enhanced and shows a hump at around 5–20 K, which is very similar to the phonon-drag humps in S_0. The same behavior also holds in S_{xx}/T.

There has been attribution of this enhancement to the topological origins [29], yet the characteristic peak temperatures in Figs. 5(b) and 5(c) have a large discrepancy from the energy of the Weyl nodes in this family (details are in the Supplemental Material, Sec. F [35]). Instead, we find that this behavior is actually related to the phonons. The broad hump in the curves of Figs. 5(b) and 5(c) can be regarded as a temperature range in which phonons scatter electrons most efficiently. Such a condition is satisfied when a typical phonon wave vector $\boldsymbol{q}$ becomes comparable to twice that of an electron wave vector ($2k_F$) [70]. The effective Debye temperature, $\Theta_D^* = 2k_F c_s \hbar/k_B$, where c_s is the sound velocity, could be used to describe such a characteristic temperature. Using k_F and c_s determined from QOs and Debye temperature [71], respectively, we estimate Θ_D^* to be 6.6, 12.3, 11.0, and 20.0 K for the four members. This is in good agreement with the peak temperature of $\nu(T)/T$ equaling 5, 15, 10, and 20 K for TaAs, TaP, NbAs, and NbP, respectively. For bismuth, the estimated Θ_D^* in the same procedure (Table I) also shows good consistency with its phonon-drag temperature [70]. The large enhancement of ν/T and S_{xx}/T at intermediate temperature in the TaAs family does point to a comparable component from phonon drag aside from the diffusive part.

In short, the large S_{xx} and S_{xy} in the TaAs family are a combined result of small Fermi energy, ultrahigh carrier mobility, and a large phonon-drag effect. Detailed information used in this part is summarized in Table I.

D. Phonon drag in thermoelectric quantum oscillations

In this section, we study the QOs observed in Figs. 1 and 2 and prove that the phonon drag also plays an important role in the thermoelectric QOs in the TaAs family. We take the QOs of TaAs as an example, which only involves one principal frequency from the electron band. Similar results are also observed in TaP (Fig. S9 in the Supplemental Material [35]). We first calculate the thermoelectric tensor $\boldsymbol{\alpha}$ and then separate the oscillatory and background parts, denoted as $\widetilde{\boldsymbol{\alpha}}$ and $\overline{\boldsymbol{\alpha}}$, respectively. The oscillatory and background parts for the electrical conductivity tensor are denoted as $\widetilde{\boldsymbol{\sigma}}$ and $\overline{\boldsymbol{\sigma}}$ as well. According to the Mott relation, the diffusive part of oscillatory $\boldsymbol{\alpha}$ should follow [11,73–75]

$$\widetilde{\boldsymbol{\alpha}}^d = \mp i\frac{\pi k_B}{e}\frac{D'(\mathbb{X})}{D(\mathbb{X})}\widetilde{\boldsymbol{\sigma}} = \beta\widetilde{\boldsymbol{\sigma}}, \tag{12}$$

with the upper sign (negative) for electrons. Here $D(\mathbb{X}) = \mathbb{X}/\sinh\mathbb{X}$ is the standard thermal damping factor in the Lifshitz-Kosevich formula, with $\mathbb{X} = alX$, $a = 2\pi^2 k_B/e\hbar$, $X = m^*T/B$, m^* being the cyclotron mass, and l the harmonic number. If we associate $\widetilde{\boldsymbol{\sigma}}$ with the density of states (g), the diagonal component could be further expressed as [76]

$$\widetilde{\alpha}_{xx}^d = \frac{5}{2}\beta D(\mathbb{X})\overline{\sigma}_{xx}\frac{\widetilde{g}}{\overline{g}}. \tag{13}$$

We plot $\widetilde{\alpha}_{xx}$ of TaAs together with the diffusive part calculated by Eq. (12) in Fig. 7(a). The magnitude of $\widetilde{\sigma}_{xx}|\beta|$ is in surprisingly good agreement with $\widetilde{\alpha}_{xx}$, suggesting a dominant diffusive contribution. In contrast, $\widetilde{\alpha}_{xy}$ surpasses $\widetilde{\sigma}_{xy}|\beta|$ by 30 times in Fig. 7(b) in a strong magnetic field. We notice that the magnitude of $\widetilde{\alpha}_{xy}$ at 5 K is roughly five times larger than that of $\widetilde{\alpha}_{xx}$, whereas the amplitude of $\widetilde{\sigma}_{xy}$ is sixfold smaller than that of $\widetilde{\sigma}_{xx}$ at 7 T.

One plausible explanation for the extremely large $\widetilde{\alpha}_{xy}$ is the correction near the quantum limit in 3D systems [43,44]. It was suggested that α_{xy}^d will develop asymmetric peaks, with the peak position aligned with that of $\widetilde{\sigma}_{xx}$ under extremely low temperature and intense magnetic field. Bergman *et al.* [43] computed the peak value for α_{xy}^d under such conditions,

$$\alpha_{xy}^d \approx -\frac{2e}{h^2}k_B\sqrt{2k_B T m_z}, \tag{14}$$

with m_z being the effective mass along the field direction. Note that in Eq. (14), the only variable is the temperature. The peak value of α_{xy}^d inferred from Eq. (14) is $0.05\sqrt{T(K)}$ A/K m in strong field even when free-electron mass is adopted, which is in the same order of $\widetilde{\sigma}_{xy}|\beta|$ and much less than our experimental results. Our estimation demonstrates that the diffusive part is not enough to account for the total $\widetilde{\alpha}_{xy}$.

Another possible explanation to span the huge difference is the influence from the phonon-drag effect. To analyze the phonon-drag-induced QOs, some simplification is needed. Following Refs. [64,68], we rewrite Eq. (10) as

$$\overline{\boldsymbol{\alpha}}^g = \overline{\boldsymbol{\sigma}}S_g^0, \tag{15}$$

when QOs are not considered. Here the classical effect of the Lorentz force is included through $\overline{\boldsymbol{\sigma}}$, while details of the electron-phonon scattering are included simultaneously in S_g^0, the zero-field phonon-drag Seebeck coefficient.

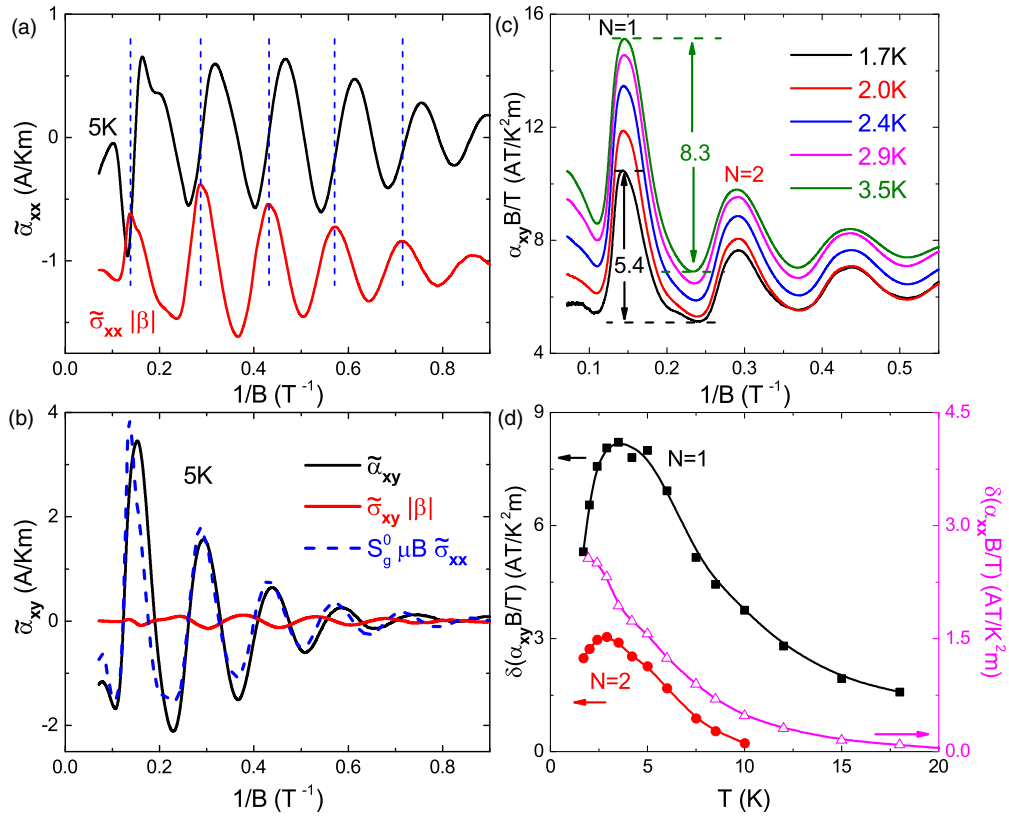

FIG. 7. (a) $\tilde{\alpha}_{xx}$ at 5 K for TaAs and corresponding $\tilde{\sigma}_{xx}|\beta|$ at 5 K (shifted for clarity). For brevity, the contribution from higher harmonics is not treated separately. Note the similar magnitudes and 1/4 phase shift. (b) $\tilde{\alpha}_{xy}$ at 5 K and $\tilde{\sigma}_{xy}|\beta|$ at 5 K for comparison. Unlike the case in (a), $\tilde{\sigma}_{xy}|\beta|$ is way smaller than $\tilde{\alpha}_{xy}$. Dashed line is $S_g^0\mu B\tilde{\sigma}_{xx}$ at 5 K, with S_g^0 taken to be 2.5 μV/K. (c) $\alpha_{xy}B/T$ at low temperatures. The height of the $N=1$ peak damps with decreasing temperature below 4 K. (d) Left scale: peak height for $\alpha_{xy}B/T$, plotted against temperature. The magenta curve is the peak height for $\alpha_{xx}B/T$ at 7.6 T, showing a monotonically decreasing feature.

When magnetic quantization is considered, the probability of electron-phonon scattering is supposed to oscillate with the density of states (DOS), and Eq. (15) is modified to be

$$\boldsymbol{\alpha}^g = \overline{\sigma} S_g^0\left(1+\gamma\frac{\tilde{g}}{\overline{g}}\right), \quad \tilde{\boldsymbol{\alpha}}^g = \gamma S_g^0\overline{\sigma}\frac{\tilde{g}}{\overline{g}}, \tag{16}$$

where γ is a constant in the order of unity.

From Eqs. (13) and (16), we can compare the contribution of phonon drag with the diffusive part in diagonal $\tilde{\alpha}_{xx}$,

$$\tilde{\alpha}_{xx}^g/\tilde{\alpha}_{xx}^d = \frac{2\gamma}{5D(\mathbb{X})}\left(S_g^0/\beta\right). \tag{17}$$

At low temperature and strong field, the coefficient $D(\mathbb{X})\sim 1$, and S_g^0 for electrons is estimated to be much less than 10 μV/K at 5 K. As a comparison, $|\beta|$ is a fairly large coefficient, being 117 μV/K at 5 K, 7 T, and gradually approaching 271 μV/K for large $\mathbb{X}$. Equation (17), therefore, indicates a negligible contribution of phonon drag (an order smaller than $\tilde{\alpha}_{xx}^d$) in total $\tilde{\alpha}_{xx}$. Moreover, we notice that the two sets of QOs in Fig. 7(a) have 1/4 phase shift. This is consistent with the fact that the QOs in the diffusive part acquire a $-i$ phase (inside β) with respect to $\tilde{\sigma}_{xx}$ for electrons. As a comparison, the phonon-drag contributed QOs are in phase with $\tilde{\sigma}_{xx}$.

Now we compare the off-diagonal $\tilde{\alpha}_{xy}^g$ and in-diagonal $\tilde{\alpha}_{xx}^g$ in a strong magnetic field. We have $\tilde{\alpha}_{xy}^g/\tilde{\alpha}_{xx}^g = \overline{\sigma}_{xy}/\overline{\sigma}_{xx} = \mu B$ according to Eq. (16). We note that $\tilde{\alpha}_{xy}^g$ is enhanced by a factor of μB compared to $\tilde{\alpha}_{xx}^g$. Even if $\tilde{\alpha}_{xx}^g$ is negligible in total $\tilde{\alpha}_{xx}$, $\tilde{\alpha}_{xy}^g$ may still be very large in a strong field due to the high mobility (over 50 m^2/V s for TaAs) of the electrons.

Then we weigh $\tilde{\alpha}_{xy}^g$ and $\tilde{\alpha}_{xy}^d$ in the total $\tilde{\alpha}_{xy}$ in a general way. Using Eq. (12) for the diffusive part, with $\tilde{\sigma}_{xy}\propto\frac{\overline{\sigma}_{xx}}{\mu B}\frac{\tilde{g}}{\overline{g}}$ [74], and Eq. (16) for the phonon-drag part, we have

$$\frac{|\tilde{\alpha}_{xy}^g|}{|\tilde{\alpha}_{xy}^d|}\propto\left|\frac{S_g^0}{\beta}\right|\mu^2B^2. \tag{18}$$

The carrier mobility can easily reach over 400 m^2/V s [72] in semimetals like bismuth. For the TaAs family, the mobility for the light carriers ranges from 8.5 to 55 m^2/V s (Table I). Even a tiny S_g^0 is expected to have a tremendous impact on the total $\tilde{\alpha}_{xy}$ for these semimetals under high fields. This large phonon-drag contribution in $\tilde{\alpha}_{xy}$ also explains the sharp, sawlike Nernst QOs in TaAs and TaP. We expect that the large Nernst QOs observed in other semimetals [7,41,42] may also have a bearing on the phonon-drag effect.

We can roughly reproduce the profile of $\tilde{\alpha}_{xy}$ with Eq. (16) by assuming some reasonable parameters ($S_g^0 = 2.5$ μV/K, $\gamma = 1$) and disregarding the damping factor. As shown in Fig. 7(b), the peak size and profile of $\tilde{\alpha}_{xy}^g \simeq S_g^0\mu B\tilde{\sigma}_{xx}$ match the experimental $\tilde{\alpha}_{xy}$ very well.

Finally, we analyze the temperature dependence of the oscillation amplitude for the last few Landau levels in order

to demonstrate other signatures of the phonon-drag effect in QOs. As shown in Figs. 7(c) and 7(d), the peak height of $\alpha_{xy}B/T$ for the last two Landau levels shows a maximum at intermediate temperature. As a comparison, the peak height of $\alpha_{xx}B/T$ drops monotonically with increasing temperature. The different temperature dependence can be well understood if we assume they originate from different effects. In $\widetilde{\alpha}_{xy}B/T$, the phonon-drag part $\widetilde{\alpha}^{g}_{xy}B/T$ dominates. Since it is proportional to S^{0}_{g}/T at a fixed magnetic field, $\widetilde{\alpha}_{xy}B/T$ will show a maximum at an intermediate temperature. In contrast, the diffusive part dominates in $\widetilde{\alpha}_{xx}B/T$ and the size of $\widetilde{\alpha}^{d}_{xx}B/T$ depends on β/T. Because β/T decreases monotonically with increasing temperature, $\widetilde{\alpha}_{xx}B/T$ reaches a maximum at the lowest temperature.

E. Thermoelectricity in a strong magnetic field

In this section, we discuss the thermoelectricity of the TaAs family in a strong-field, extreme quantum limit (EQL) when $v_F\sqrt{\hbar|eB|} \gg k_BT$ and $v_F\sqrt{\hbar|eB|} \gg \epsilon_F$ [9]. A nonsaturating magnetothermopower and a "quantized" thermoelectric Hall conductivity were theoretically proposed above the EQL for Dirac and Weyl semimetals [9,10]. There have been reports of such observations in $ZrTe_5$ [77] and TaP [31].

The "quantized" thermoelectric Hall conductivity is due to a linear field-dependent DOS in the zeroth Landau level in a linearly dispersive band. A diffusive α_{xy} which is independent of field is expected above the EQL [9],

$$\alpha^{\text{ideal}}_{xy}/T = -\frac{1}{12}\frac{ek_B^2}{\hbar^2}\frac{N_f}{v_F}, \tag{19}$$

where N_f is the number of Weyl nodes, and v_F is the corresponding Fermi velocity along the z direction. There are 8 W_1 nodes and 16 W_2 nodes in TaAs, and the corresponding v_z can be found in Ref. [22]. We plot α_{xy}/T of TaAs at representative temperatures in Fig. 8, together with the calculated $\alpha^{\text{ideal}}_{xy}/T$ from Eq. (19).

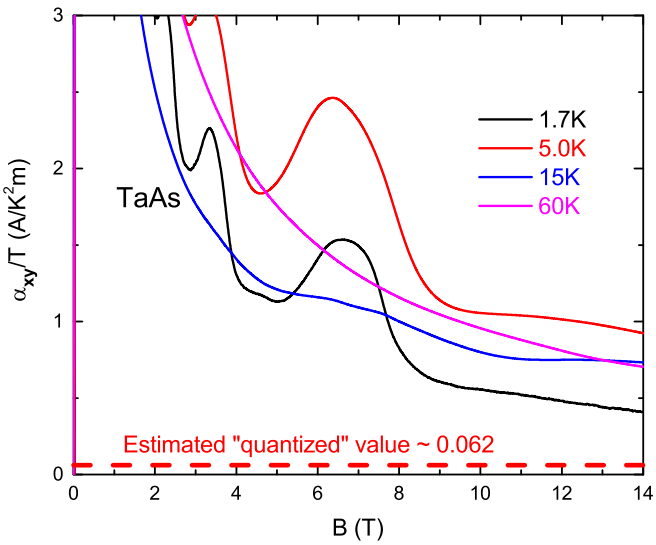

FIG. 8. α_{xy}/T for TaAs at representative temperatures. The quantized value expected by Eq. (19) in EQL is by far smaller than the experimentally observed value.

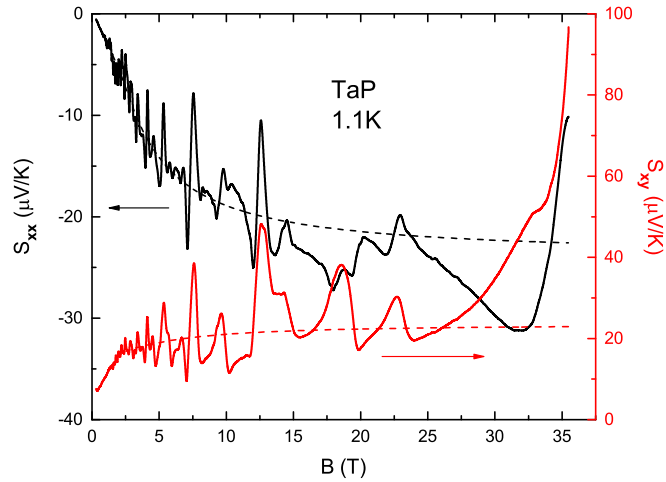

FIG. 9. S_{xx} and S_{xy} for TaP under high magnetic field. Dashed lines denote nonoscillatory backgrounds.

As the Fermi velocity is around 0.5×10^5 and 2×10^5 m/s for W_1 and W_2 in TaAs, respectively, the $\alpha^{\text{ideal}}_{xy}/T$ is estimated as 0.06 A/K^2 m. This value is an order smaller than measurement. Note that at 15 K and 14 T, the condition for the EQL is still satisfied. Moreover, the absence of the plateaulike feature at high field indicates that the main part still consists of conventional signals changing as $1/B$. A large discrepancy is also seen in TaP, NbAs, and NbP (Fig. S10).

As shown in Figs. 1(a) and 2(a), the S_{xx} in TaAs does not show any trend of increasing with magnetic field at low temperature. We also measured the thermoelectricity for TaP up to 35 T at 1.1 K (Fig. 9). There is no sign of nonsaturating S_{xx} as well. In short, we do *not* observe the "quantized" thermoelectric Hall conductivity and nonsaturating magnetothermopower in the TaAs family in the present experimental conditions.

V. CONCLUSION

In summary, our studies on the thermoelectric transport properties in the prototype Weyl semimetal TaAs family reveal several important facts. First, the large Seebeck and Nernst signals under magnetic field are a result of combined effects including small Fermi energy, ultrahigh carrier mobility, and large phonon-drag effect in these semimetals. In particular, the phonon drag plays an important role in the large thermoelectric signal at intermediate temperatures and the unusual QOs in the off-diagonal thermoelectric tensor. Secondly, we discern signatures of anomalous thermoelectric Hall conductivity as a Berry-curvature-field effect in TaAs in which the Weyl nodes are properly situated in the energy scale.

Thermoelectric properties in topological semimetals are complex because the topological effects often get entangled with ordinary effect and inelastic scattering processes. Our work highlights an effective strategy for discerning the origins of the magnetothermoelectric signals. We believe that a comprehensive consideration of the interplay of electron and phonon is crucial for understanding the thermoelectric effect in topological materials.

ACKNOWLEDGMENTS

We thank Cheng-Long Zhang for his guidance during the early instrumental setup and later discussion on the ANE of TaAs. This work is supported by the National Natural Science Foundation of China Grants No. U1832214, No. 11774007, No. U2032213, No. 11774352, and No. 12104461, the National Key R & D Program of China (2018YFA0305601) and the strategic Priority Research Program of Chinese Academy of Sciences Grant No. XDB28000000. X.X. acknowledges support from the China Postdoctoral Science Foundation Grant No. 2020M682056, Anhui Postdoctoral Foundation Grant No. 2020B472, Anhui Provincial Natural Science Foundation Grant No. 2108085QA23, the HFIPS Director's Fund Grant No. YZJJ2021QN28, and Special Research Assistant Program, Chinese Academy of Sciences. LNCMI-CNRS is a member of the European Magnetic Field Laboratory (EMFL).

[1] H. J. Goldsmid, *Introduction to Thermoelectricity* (Springer, Berlin, 2010), Vol. 121.
[2] J. M. Ziman, *Electrons and Phonons: The Theory of Transport Phenomena in Solids* (Oxford University Press, Oxford, 2001).
[3] M. Z. Hasan and C. L. Kane, Rev. Mod. Phys. **82**, 3045 (2010).
[4] X.-L. Qi and S.-C. Zhang, Rev. Mod. Phys. **83**, 1057 (2011).
[5] A. Burkov, Annu. Rev. Condens. Matter Phys. **9**, 359 (2018).
[6] B. BBradlyn, J. Cano, Z. Wang, M. G. Vergniory, C. Felser, R. J. Cava, and B. A. Bernevig, Science **353**, aaf5037 (2016).
[7] T. Liang, J. Lin, Q. Gibson, T. Gao, M. Hirschberger, M. Liu, R. J. Cava, and N. P. Ong, Phys. Rev. Lett. **118**, 136601 (2017).
[8] M. Hirschberger, S. Kushwaha, Z. Wang, Q. Gibson, S. Liang, C. A. Belvin, B. A. Bernevig, R. J. Cava, and N. P. Ong, Nat. Mater. **15**, 1161 (2016).
[9] V. Kozii, B. Skinner, and L. Fu, Phys. Rev. B **99**, 155123 (2019).
[10] B. Skinner and L. Fu, Sci. Adv. **4**, eaat2621 (2018).
[11] R. Fletcher, J. Low Temp. Phys. **43**, 363 (1981).
[12] M. Matusiak, J. Cooper, and D. Kaczorowski, Nat. Commun. **8**, 15219 (2017).
[13] X. Xu, Z. Kang, T.-R. Chang, H. Lin, G. Bian, Z. Yuan, Z. Qu, J. Zhang, and S. Jia, Phys. Rev. B **99**, 104516 (2019).
[14] X. Xu, X. Wang, T. A. Cochran, D. S. Sanchez, G. Chang, I. Belopolski, G. Wang, Y. Liu, H.-J. Tien, X. Gui, W. Xie, M. Z. Hasan, T.-R. Chang, and S. Jia, Phys. Rev. B **100**, 045104 (2019).
[15] G. Sharma, P. Goswami, and S. Tewari, Phys. Rev. B **93**, 035116 (2016).
[16] G. Sharma, C. Moore, S. Saha, and S. Tewari, Phys. Rev. B **96**, 195119 (2017).
[17] Y. Gurevich and O. Mashkevich, Phys. Rep. **181**, 327 (1989).
[18] D. K. C. MacDonald, *Thermoelectricity: An Introduction to the Principles* (Courier, Mineola, New York, 2006).
[19] K. Behnia, *Fundamentals of Thermoelectricity* (Oxford University Press, Oxford, 2015).
[20] S. Jia, S.-Y. Xu, and M. Z. Hasan, Nat. Mater. **15**, 1140 (2016).
[21] B. Yan and C. Felser, Annu. Rev. Condens. Matter Phys. **8**, 337 (2017).
[22] C.-C. Lee, S.-Y. Xu, S.-M. Huang, D. S. Sanchez, I. Belopolski, G. Chang, G. Bian, N. Alidoust, H. Zheng, M. Neupane, B. Wang, A. Bansil, M. Z. Hasan, and H. Lin, Phys. Rev. B **92**, 235104 (2015).
[23] C.-L. Zhang, S.-Y. Xu, I. Belopolski, Z. Yuan, Z. Lin, B. Tong, G. Bian, N. Alidoust, C.-C. Lee, S.-M. Huang, T.-R. Chang, G. Chang, C.-H. Hsu, H.-T. Jeng, M. Neupane, D. S. Sanchez, H. Zheng, J. Wang, H. Lin, C. Zhang, H.-Z. Lu, S.-Q. Shen, T. Neupert, M. Zahid Hasan, and S. Jia, Nat. Commun. **7**, 10735 (2016).
[24] X. Huang, L. Zhao, Y. Long, P. Wang, D. Chen, Z. Yang, H. Liang, M. Xue, H. Weng, Z. Fang, X. Dai, and G. Chen, Phys. Rev. X **5**, 031023 (2015).
[25] C. Shekhar, A. K. Nayak, Y. Sun, M. Schmidt, M. Nicklas, I. Leermakers, U. Zeitler, Y. Skourski, J. Wosnitza, Z. Liu, Y. Chen, W. Schnelle, H. Borrmann, Y. Grin, C. Felser, and B. Yan, Nat. Phys. **11**, 645 (2015).
[26] Z. Wang, Y. Zheng, Z. Shen, Y. Lu, H. Fang, F. Sheng, Y. Zhou, X. Yang, Y. Li, C. Feng, and Z.-A. Xu, Phys. Rev. B **93**, 121112(R) (2016).
[27] F. Arnold, C. Shekhar, S.-C. Wu, Y. Sun, R. D. dos Reis, N. Kumar, M. Naumann, M. O. Ajeesh, M. Schmidt, A. G. Grushin, J. H. Bardarson, M. Baenitz, D. Sokolov, H. Borrmann, M. Nicklas, C. Felser, E. Hassinger, and B. Yan, Nat. Commun. **7**, 11615 (2016).
[28] U. Stockert, R. D. Dos Reis, M. O. Ajeesh, S. J. Watzman, M. Schmidt, C. Shekhar, J. P. Heremans, C. Felser, M. Baenitz, and M. Nicklas, J. Phys.: Condens. Matter **29**, 325701 (2017).
[29] S. J. Watzman, T. M. McCormick, C. Shekhar, S.-C. Wu, Y. Sun, A. Prakash, C. Felser, N. Trivedi, and J. P. Heremans, Phys. Rev. B **97**, 161404(R) (2018).
[30] F. Caglieris, C. Wuttke, S. Sykora, V. Süss, C. Shekhar, C. Felser, B. Büchner, and C. Hess, Phys. Rev. B **98**, 201107(R) (2018).
[31] F. Han, N. Andrejevic, T. Nguyen, V. Kozii, Q. T. Nguyen, T. Hogan, Z. Ding, R. Pablo-Pedro, S. Parjan, B. Skinner, A. Alatas, E. Alp, S. Chi, J. Fernandez-Baca, S. Huang, L. Fu, and M. Li, Nat. Commun. **11**, 6167 (2020).
[32] C.-L. Zhang, Z. Yuan, Q.-D. Jiang, B. Tong, C. Zhang, X. C. Xie, and S. Jia, Phys. Rev. B **95**, 085202 (2017).
[33] C. Zhang, C. Guo, H. Lu, X. Zhang, Z. Yuan, Z. Lin, J. Wang, and S. Jia, Phys. Rev. B **92**, 041203(R) (2015).
[34] N. J. Ghimire, Y. Luo, M. Neupane, D. J. Williams, E. D. Bauer, and F. Ronning, J. Phys.: Condens. Matter **27**, 152201 (2015).
[35] See Supplemental Material at http://link.aps.org/supplemental/10.1103/PhysRevB.104.115164 for experimental and theoretical details as well as additional figures and discussions, which includes Refs. [36–40].
[36] F. Freibert, T. W. Darling, A. Migliori, and S. A. Trugman, in *Semiconductors and Semimetals* (Elsevier, Amsterdam, 2001), Vol. 70, pp. 207–244.
[37] C.-L. Zhang, B. Tong, Z. Yuan, Z. Lin, J. Wang, J. Zhang, C.-Y. Xi, Z. Wang, S. Jia, and C. Zhang, Phys. Rev. B **94**, 205120 (2016).
[38] C.-L. Zhang, S.-Y. Xu, C. M. Wang, Z. Lin, Z. Z. Du, C. Guo, C.-C. Lee, H. Lu, Y. Feng, S.-M. Huang *et al.*, Nat. Phys. **13**, 979 (2017).

[39] Y. Luo, N. J. Ghimire, M. Wartenbe, H. Choi, M. Neupane, R. D. McDonald, E. D. Bauer, J. Zhu, J. D. Thompson, and F. Ronning, Phys. Rev. B **92**, 205134 (2015).

[40] J. Klotz, S.-C. Wu, C. Shekhar, Y. Sun, M. Schmidt, M. Nicklas, M. Baenitz, M. Uhlarz, J. Wosnitza, C. Felser, and B. Yan, Phys. Rev. B **93**, 121105 (2016).

[41] K. Behnia, M.-A. Méasson, and Y. Kopelevich, Phys. Rev. Lett. **98**, 166602 (2007).

[42] Z. Zhu, H. Yang, B. Fauqué, Y. Kopelevich, and K. Behnia, Nat. Phys. **6**, 26 (2010).

[43] D. L. Bergman and V. Oganesyan, Phys. Rev. Lett. **104**, 066601 (2010).

[44] I. A. Luk'yanchuk, A. A. Varlamov, and A. V. Kavokin, Phys. Rev. Lett. **107**, 016601 (2011).

[45] A. Akrap, A. Ubaldini, E. Giannini, and L. Forró, Europhys. Lett. **107**, 57008 (2014).

[46] J. P. Heremans, C. M. Thrush, and D. T. Morelli, Phys. Rev. Lett. **86**, 2098 (2001).

[47] J. P. Heremans, C. M. Thrush, and D. T. Morelli, Phys. Rev. B **65**, 035209 (2001).

[48] J. H. Mangez, J. P. Issi, and J. Heremans, Phys. Rev. B **14**, 4381 (1976).

[49] Z. Zhu, X. Lin, J. Liu, B. Fauqué, Q. Tao, C. Yang, Y. Shi, and K. Behnia, Phys. Rev. Lett. **114**, 176601 (2015).

[50] K. Behnia, J. Phys.: Condens. Matter **21**, 113101 (2009).

[51] D. Xiao, M.-C. Chang, and Q. Niu, Rev. Mod. Phys. **82**, 1959 (2010).

[52] X. Li, L. Xu, L. Ding, J. Wang, M. Shen, X. Lu, Z. Zhu, and K. Behnia, Phys. Rev. Lett. **119**, 056601 (2017).

[53] C. Wuttke, F. Caglieris, S. Sykora, F. Scaravaggi, A. U. B. Wolter, K. Manna, V. Süss, C. Shekhar, C. Felser, B. Büchner, and C. Hess, Phys. Rev. B **100**, 085111 (2019).

[54] A. Sakai, Y. P. Mizuta, A. A. Nugroho, R. Sihombing, T. Koretsune, M.-T. Suzuki, N. Takemori, R. Ishii, D. Nishio-Hamane, R. Arita, P. Goswami, and S. Nakatsuji, Nat. Phys. **14**, 1119 (2018).

[55] L. Xu, X. Li, L. Ding, T. Chen, A. Sakai, B. Fauqué, S. Nakatsuji, Z. Zhu, and K. Behnia, Phys. Rev. B **101**, 180404(R) (2020).

[56] H. Yang, W. You, J. Wang, J. Huang, C. Xi, X. Xu, C. Cao, M. Tian, Z.-A. Xu, J. Dai, and Y. Li, Phys. Rev. Mater. **4**, 024202 (2020).

[57] L. Ding, J. Koo, L. Xu, X. Li, X. Lu, L. Zhao, Q. Wang, Q. Yin, H. Lei, B. Yan, Z. Zhu, and K. Behnia, Phys. Rev. X **9**, 041061 (2019).

[58] H. Zhang, C. Q. Xu, and X. Ke, Phys. Rev. B **103**, L201101 (2021).

[59] T. Liang, J. Lin, Q. Gibson, S. Kushwaha, M. Liu, W. Wang, H. Xiong, J. A. Sobota, M. Hashimoto, P. S. Kirchmann, Z.-X. Shen, R. J. Cava, and N. P. Ong, Nat. Phys. **14**, 451 (2018).

[60] P. Wang, C.-w. Cho, F. Tang, P. Wang, W. Zhang, M. He, G. Gu, X. Wu, Y. Shao, and L. Zhang, Phys. Rev. B **103**, 045203 (2021).

[61] M. N. Ali, J. Xiong, S. Flynn, J. Tao, Q. D. Gibson, L. M. Schoop, T. Liang, N. Haldolaarachchige, M. Hirschberger, N. P. Ong, and R. J. Cava, Nature (London) **514**, 205 (2014).

[62] J. Weischenberg, F. Freimuth, S. Blügel, and Y. Mokrousov, Phys. Rev. B **87**, 060406(R) (2013).

[63] J. Mutch, X. Ma, C. Wang, P. Malinowski, J. Ayres-Sims, D. Xiao, M. Yankowitz, and J.-H. Chu, arXiv:2101.02681.

[64] X. Zianni, P. N. Butcher, and M. J. Kearney, Phys. Rev. B **49**, 7520 (1994).

[65] H. P. R. Frederikse, Phys. Rev. **92**, 248 (1953).

[66] J.-P. Issi, Aust. J. Phys. **32**, 585 (1979).

[67] Z. Li, H. Chen, S. Jin, D. Gan, W. Wang, L. Guo, and X. Chen, Cryst. Growth Des. **16**, 1172 (2016).

[68] B. Tieke, R. Fletcher, J. C. Maan, W. Dobrowolski, A. Mycielski, and A. Wittlin, Phys. Rev. B **54**, 10565 (1996).

[69] K. Behnia and H. Aubin, Rep. Prog. Phys. **79**, 046502 (2016).

[70] C. Uher and W. P. Pratt Jr., J. Phys. F **8**, 1979 (1978).

[71] L. Liu, Z.-Q. Wang, C.-E. Hu, Y. Cheng, and G.-F. Ji, Solid State Commun. **263**, 10 (2017).

[72] K. Behnia, M.-A. Méasson, and Y. Kopelevich, Phys. Rev. Lett. **98**, 076603 (2007).

[73] R. Fletcher, Phys. Rev. B **28**, 1721 (1983).

[74] P. T. Coleridge, R. Stoner, and R. Fletcher, Phys. Rev. B **39**, 1120 (1989).

[75] R. Fletcher, P. T. Coleridge, and Y. Feng, Phys. Rev. B **52**, 2823 (1995).

[76] D. Shoenberg, *Magnetic Oscillations in Metals* (Cambridge University Press, Cambridge, 2009).

[77] W. Zhang, P. Wang, B. Skinner, R. Bi, V. Kozii, C.-W. Cho, R. Zhong, J. Schneeloch, D. Yu, G. Gu, L. Fu, X. Wu, and L. Zhang, Nat. Commun. **11**, 1046 (2020).